Dynamic Hydrogels

International Edition: DOI: 10.1002/anie.201913574
German Edition: DOI: 10.1002/ange.201913574

Macroscopic Self-Evolution of Dynamic Hydrogels to Create Hollow Interiors

Lu Han[+], Yijun Zheng[+], Hao Luo[+], Jun Feng, Roxanne Engstler, Lulu Xue, Guangyin Jing, Xu Deng,* Aránzazu del Campo, and Jiaxi Cui**

Abstract: *A solid-to-hollow evolution in macroscopic structures is challenging in synthetic materials. A fundamentally new strategy is reported for guiding macroscopic, unidirectional shape evolution of materials without compromising the material's integrity. This strategy is based on the creation of a field with a "swelling pole" and a "shrinking pole" to drive polymers to disassemble, migrate, and resettle in the targeted region. This concept is demonstrated using dynamic hydrogels containing anchored acrylic ligands and hydrophobic long alkyl chains. Adding water molecules and ferric ions (Fe^{3+}) to induce a swelling–shrinking field transforms the hydrogels from solid to hollow. The strategy is versatile in the generation of various closed hollow objects (for example, spheres, helix tubes, and cubes with different diameters) for different applications.*

Living organisms can vary their macroscopic shapes to achieve vital biological functions via a series of precise mass transports and reconfigurations.[1–6] For instance, *Mimosa* plant species can modulate water movement from some cells to others in pulvini (the enlarged section at the base of leaf stalks) to stimulate folding/unfolding of leaflets.[7] In the case that the transported mass is irreversibly integrated, a permanent shape is created, such as flower opening[8] and tree trunk hollowing.[9] To enable the mass transport and conversion, subtle gradient fields,[10] such as the ion concentration gradient in plant pulvini,[11] are frequently built to drive molecular components to disassemble, transfer, and re-bond into new architectures at precise locations where new equilibrium states form.[12] The processes are coupled and self-organized. Many synthetic material systems based on molecular reconfiguration are able to vary their shapes and properties, including shape-memory materials,[13–15] liquid crystal elastomers,[16–18] systems with self-healing ability[19]/environmental adaptivity[20]/self-formation capability,[21] and others.[22–26] Some of them are quite sophisticated in macroscopic deformation,[13] but they are designed to return to their original shapes and only involve in some relatively simple changes, such as contracting, twisting, and bending. It is still challenging to realize macroscopic shape-evaluation-like transitions from solid to closed hollow structures. Even hollow structures are essential for many functions, from mass delivery to mechanical property modulation.[27,28]

Herein, we present a new strategy for regulating macroscopic evolution of polymer-based dynamic hydrogels from solid to closed hollow structures. The strategy leverages the creation of a swelling–shrinking field to guide the disassembly, long-distance diffusion, and re-association of cross-linked polymers. We demonstrated this concept by using a hydrogel system that is cross-linked by the weak hydrophobic association interaction of stearyl methacrylate (C_{18}) units but contains abundant acrylic side chains for forming strong complexes with ferric ions (Fe^{3+}, Figure 1a; Supporting Information, Figure S1).[29] The hydrogels were firstly prepared by micellar copolymerization of C_{18}, acrylamide, and acrylate acid in the presence of sodium dodecyl sulfate (SDS) surfactant (Supporting Information). As-prepared hydrogels possess a well-defined shape but are fully dynamic, showing fast self-healing ability and excellent stretchability (Figure S2).

A Fe^{3+} solution was then used to create a swelling–shrinking field to induce the hydrogel's shape evolution. Figures 1a,b present a schematic and the practical evaluation process, respectively, with a hydrogel rod as an example. When the opaque hydrogel was immersed in a $FeCl_3$ solution, both Fe^{3+} ions and water molecules diffuse into the hydrogel (Figure 1a i→ii and Figure 1b i→ii). Water swells the hydrogel and makes it transparent, whereas Fe^{3+} dyes the hydrogel and causes shrinkage because of the ionic cross-linking effect of Fe^{3+} with carboxy groups in hydrogels (Figure S3). Water

[*] Dr. L. Han,[+] L. Xue, Prof. X. Deng, Dr. J. Cui
Institute of Fundamental and Frontier Science,
University of Electronic Science and Technology of China
Chengdu 610054 (China)
E-mail: dengxu@uestc.edu.cn
Jiaxi.Cui@leibniz-inm.de
Dr. L. Han,[+] Dr. Y. Zheng,[+] J. Feng, R. Engstler, Prof. A. del Campo, Dr. J. Cui
INM—Leibniz Institute for New Materials,
Campus D2 2, Saarbrücken 66123 (Germany)
Dr. Y. Zheng[+]
School of Physical Science and Technology, ShanghaiTech University
Shanghai, 201210 (China)
Prof. A. del Campo
Chemistry Department, Saarland University
66123, Saarbrücken (Germany)
Dr. H. Luo,[+] Prof. G. Jing
School of Physics, Northwest University
Xi'an 710127 (China)
E-mail: jing@nwu.edu.cn
[+] These authors contributed equally to this work.
Supporting information and the ORCID identification number(s) for the author(s) of this article can be found under: https://doi.org/10.1002/anie.201913574.

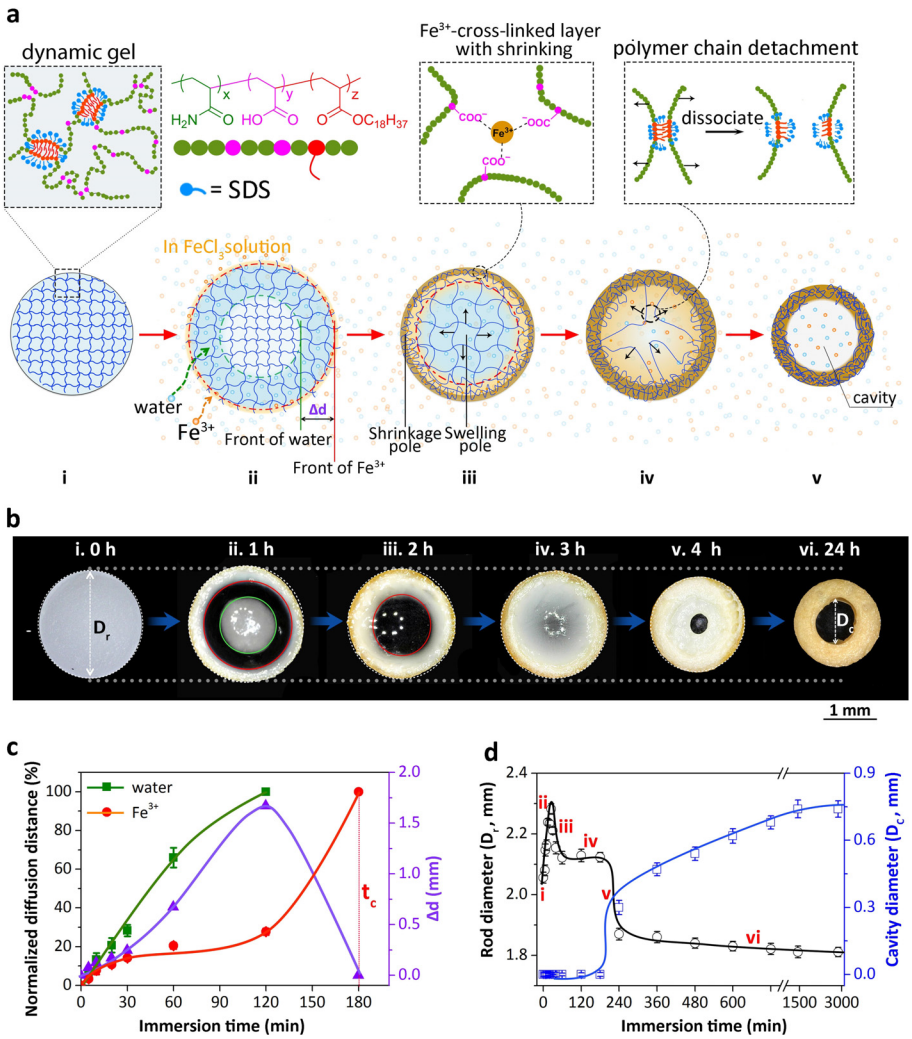

Figure 1. Self-evaluation of dynamic hydrogels from solid to hollow. a) Schematic depicting the hollowing process. (i) The PAAc-PAMm hydrogel is cross-linked by hydrophobic association interactions of C_{18} units. It is (ii) swollen by water and then (iii) deswollen by Fe^{3+}-induced cross-linking. The shrinkage pole is defined as the rear of the Fe^{3+}-induced cross-linking. Polymer chains move from the inside to the outside, in which (iv) dissociation of the hydrophobic association interaction occurs, leading to (v) a macroscopic cavitation. b) Typical time-dependent morphological evolution of the cross section of the PAAc-PAMm hydrogel rod during immersion in a 0.06 M $FeCl_3$ solution. The front of water (green circles) and Fe^{3+} (red circles) diffusing in. c) Plots of the fronts of water and Fe^{3+} that are diffusing in, as well as their band (Δd, shown in (a ii)) during immersion. The critical time when the front of Fe^{3+} arrives to the center of the rod is denoted by t_c. d) A plot of the rod diameter change of the hydrogel and cavity diameter during the hollowing process. The data in (c) and (d) were obtained by three independent measurements. Error bars are the standard error of the mean (s.e.m.).

molecules diffuse significantly faster than Fe^{3+} (Figure 1 c), forming a swelling front and a shrinking rear (Figure 1 a ii and Figure 1 b ii). The faster water-induced swelling leads to an increase in diameter at first (Figure 1 b i→ii and Figure 1 d ii). The subsequent Fe^{3+}-induced shrinking effect exceeds the water-swelling effect, and the diameter of the hydrogel rod decreases (Figure 1 a ii→iii, Figure 1 b ii→iii, and Figure 1 d iii). As a result of the synergistic effect, polymer chains collapsed in the shrinking pole (outer layer) but extended in the swelling pole (inside layer); the non-covalently cross-linked polymer chains escaped from the inside and migrated toward the shell (Figure 1 a iv). Such polymer replenishment balanced the shrinkage in the periphery and stopped the decrease in the diameter of the hydrogel rod (Figure 1 b iii→iv and Figure 1 d iv). With continuous transport of polymer outward under the swelling–shrinking field, macroscopic detachment occurs in the center, leading to a hollow structure (Figure 1 a iv→v, Figure 1 b iv→v, and Figure 1 d v). The swelling effect vanished in the center when polymer chains completely disassembled. Without polymer replenishment, the shell layer began to shrink again, accompanied by an increase in the cavity dimension. The cavitation depends on the coupling of Fe^{3+}-induced shrinkage and water swelling. We confirmed this by separating these two processes; that is, by immersing the as-prepared hydrogel in pure water to allow it to swell until reaching an equilibrium state, followed by treatment in a $FeCl_3$ solution, which results in a solid product (Figure S3).

A diffusion dynamics relationship was constructed to describe the cavitation process by defining the volume fractions of Fe^{3+} ions and H_2O in the hydrogel as $\Phi_i(x,t)$, where $i=1$ for ions and $i=2$ for water. The time evolution of Φ_i is obtained by the mass conservation equation, $\frac{\partial \Phi_i}{\partial t} = -\frac{\partial \Phi_i v_i}{\partial x}$, where the mean velocity $v_i(x)$ is the equilibrium Stokes velocity calculated from the balance of the diffusion gradient against the viscous drag. The copolymer with the volume fraction of $\varphi_p = 1-\Phi_1-\Phi_2$ cross-links with the inward diffusion of Fe^{3+} ions. The evolutions of Φ_1 and Φ_2 are:

$$\frac{\partial \Phi_1}{\partial_t} = -\frac{\partial \Phi_1 v_1}{\partial_x} + \beta \varphi_p \frac{\Phi_1}{\tau}, \quad \frac{\partial \Phi_2}{\partial_t} = -\frac{\partial \Phi_2 v_2}{\partial_x}, \tag{1}$$

where β is a cross-link coefficient, and τ is characteristic time controlled by the cross-linking rate. The hydrogel swells because of an increase in the water fraction Φ_2, while deswelling occurs because of the cross-link of polymers at the shell layer (that is, an increase of Φ_1). The relative volume change of the hydrogel over its initial volume V_0 is captured as,

$$\frac{\Delta V}{V_0} = -\lambda_d \beta \varphi_p \Phi_1 + \lambda_s \Phi_2, \tag{2}$$

where λ_d and λ_s parameters reflect the ability of the hydrogel to deswell and swell proportional to the concentrations of ion and water, respectively.

In the early stages of evolution, the larger diffusion coefficient of water ($D_2 \approx 4 D_1$)[30, 31] compared to Fe^{3+} results in a higher velocity v_2 and an increase of Φ_2, implying that swelling is dominant (that is, $\lambda_s \Phi_2 > \lambda_d \beta \varphi_p \Phi_1$) and that the diameter of the hydrogel rod increases. To be noticed, the diffusion coefficient of Fe^{3+} should be even lower because of the adsorption and desorption processes.[32] Following the dominant swelling, the cross-link between the copolymer with the inward Fe^{3+} accelerates and sharply shrinks the hydrogel (that is, a decrease in the characteristic cross-link time). A flat plateau is reached as a consequence of matured cross-linking near the periphery with the higher mechanical skeleton support. The continuous cross-linking in the outer part of the hydrogel creates a tension state in the copolymer networks until a final break with a sudden decrease in the diameter. The cavity is created and keeps growing with gradual shrinkage of the hydrogel.

Both the driving force generated in the swelling–shrinking field and the cohesion of the original hydrogels can be utilized to control the evolution. The Fe^{3+} concentration and C_{18} fraction in the copolymers were used to tune these two parameters, respectively (Figure S4). Increasing the Fe^{3+} concentration to enhance the field intensity enlarges the cavitary ratio in the range of 0.03–0.24 M (Figure 2a). However, further increasing the concentration reduces the cavitary ratio, and even leads to a solid product. This is explained by the fact that a high Fe^{3+} concentration leads to a strong field for polymer transport and also shortens the polymer transport time (Figure 2b). A non-monotonic relationship between the Fe^{3+} concentration and cavitary ratio was thus observed, which is also achieved by tuning the C_{18} fraction (Figure 2c). With increasing C_{18} fraction in the hydrogel (that is, hydrogel cohesion; Figure S5), the cavitary ratio increases and then decreases. We attribute the initial increase to the longer polymer transport time with a high C_{18} fraction (Figure 2d). In the higher range of C_{18} fraction (> 10 wt %),

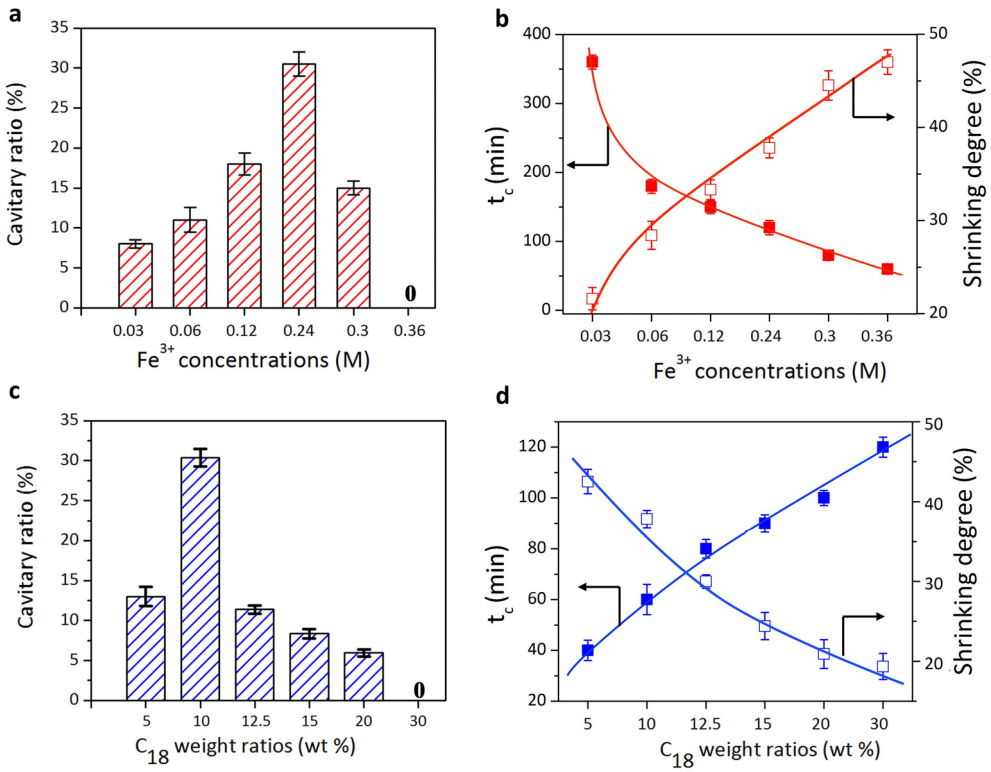

Figure 2. Variation of the hydrogel cavitary ratio with Fe^{3+} concentration/C_{18} fraction. a) Cavitary ratio vs. Fe^{3+} concentration used for hydrogel immersion. b) The critical time (t_c, which is defined in Figure 1c and represents the polymer transfer time) and the shrinking degree under different Fe^{3+} concentrations. The shrinking degree is defined as the contracting ratio in the diameter of the hydrogel rod, which represents the driving force generated in the swelling–shrinking field. The C_{18} fraction of the hydrogels in (a) and (b) is 10 wt %. c) Cavitary ratio vs. C_{18} fraction. d) The t_c and shrinking degree values with different iron concentrations. The Fe^{3+} concentration in (c) and (d) is 0.24 M. The data were obtained by three independent measurements. Error bars are s.e.m.

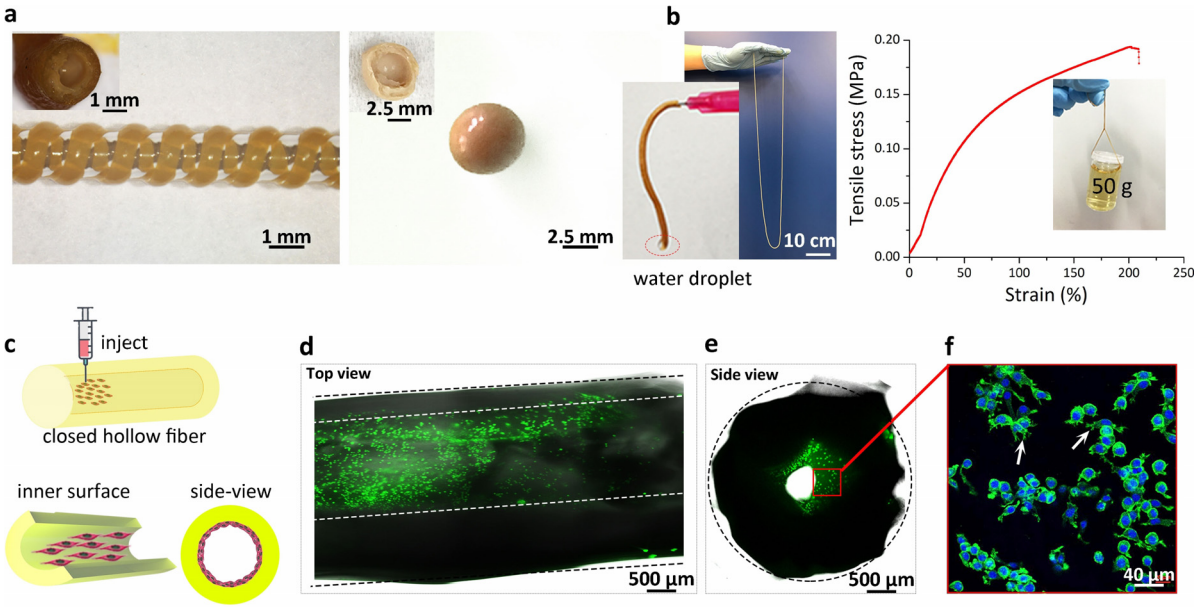

Figure 3. Fabrication of various hollow structures. a) Obtained hollow helical tube (left) and sphere (right). b) A typical long hollow fiber and its stress–strain curve. The elongation rate is 20 mm min^{-1}. Inset: the hollow and tough nature of the hollow fiber. c) Schematic of seeding cells and their growth on the inner surface of a closed hollow fiber. d) A fluorescent *z*-stack projection showing migrating L929 cells inside hollow fibers. Cells were stained by a live/dead assay kit after 7 days of culture (live cells (green), dead cells (red)). e) The cross-sectional view of the hollow fibers, which demonstrates the formation of a hollow lumen by adhered cells inside the fibers. f) Magnified image showing the morphology of cells stained with Alexa Fluor 488 phalloidin (F-actin, green) and DAPI (nuclei, blue).

cohesion-resistant molecular disassembly dominates the evolution process, and the cavitary ratio thus decreases.

The macroscopic self-evolution strategy is versatile in the generation of various closed hollow objects, including spheres, helix tubes, and cubes with different diameters (0.4–10 mm; Figures 3a,b; Figure S6). The hollow structure allows for smooth fluid transportation (Figure 3b), which indicates the presence of a whole connected interior. Long hollow fibers can be fabricated, showing the good toughness, stretchability, and underwater stability (Figure 3b; Figures S7 and S8) of the material. Interestingly, the hollow structure can return to a solid structure by washing away Fe^{3+} using aqueous solutions of a stronger Fe^{3+} complexing agent (disodium ethylenediaminetetraacetate dihydrate (Na2EDTA)). The solid structure evolves into a hollow structure once again after immersion in a Fe^{3+} solution (Figure S9).

The practical interest of hollowing hydrogels lies in the possibility of cell encapsulation within a closed hollow system.[33] We demonstrated this concept by injecting L929 fibroblasts into the hollow interiors of the hydrogel fibers (Figure 3c). The hollow fibers were stable over a timescale of at least 7 days under tissue culture conditions. Fibroblasts in hydrogel exhibit a rounded morphology and only a few colonies were observed after 1 day of culture (Figure S10). With culture durations of up to 7 days, significant cell proliferation along with fiber formation was observed, indicating that the porous nature of the polymer networks permits facile nutrient and waste transfer to support cell survival and function. A hollow lumen was developed by the adhered cells on the inner surfaces of the hollow fibers (Figures 3d,e). Phalloidin/4′,6-diamidino-2-phenylindole (DAPI) staining reveals that the cells adhered inside the fibers display a spreading morphology and a characteristic polygonal, polarized shape with extending filopdia (cytoplasmic projections) and pseudopodium (projection of a eukaryotic cell membrane; Figure 3f), which indicates that the hollow fiber can provide an optimal physiochemical microenvironment for cell–extracellular matrix (ECM) adhesion and spreading. These achievements suggest that our hollow fiber could be used as a hollow fiber bioreactor with enhanced biosafety with a closed system. It could also be used as a template for the reconstruction of fiber-shaped functional tissues.[34]

In conclusion, we have demonstrated a versatile, generic approach for spontaneous transformation of soft gel from solid to hollow structures at macroscopic levels, by creating a swelling–shrinking field to induce unidirectional polymer transportation in a dynamic material system. The cavitary degree is tunable and the cavitation process can be coupled with 3D printing technology to create scaffolds with connected/unconnected closed hollow structures for cell culture outside or inside the structure. From a general point of view, this facile yet efficient cavitation approach presents a simple method for fabricating hollow closed systems when the systems always retain solid states. We envision that this method has great potential in a variety of applications, including controlled release, additive manufacture, cell culture, fabrication of artificial organs, and protection of biologically active species.

Experimental Section

Preparation of the supramolecular hydrogels: in a typical example (Scheme S1), SDS (2.12 g) was firstly dissolved in a NaCl solution (30 mL, 0.12 M) at 40 °C to form SDS/NaCl micelles. To this solution was added C_{18} (0.13 g), followed by stirring at 40 °C for one hour to incorporate C_{18} into the micelles. AAm (1.28 g) and AAc (0.1928 mL) were then added to the mixture. After the mixture was degassed with N_2 for 30 min, ammonium persulfate (APS, 0.0737 g) and tetramethylethylenediamine (TEMED, 20 μL) were added. The mixture was stirred vigorously for 30 s, then transferred into a nitrogen-purged mold and sealed for polymerization at 66 °C for 3 h to yield the poly(acrylic acid-*co*-acrylamide) (PAAc-PAMm) hydrogel samples.

Preparation of the hydrogel rod: To quantify the degree of hollowness, the hydrogel rods with a diameter of 2 mm and a length of 4 cm were fabricated as follows. As-prepared hydrogels were heated to obtain viscous solutions, which were then injected into syringes. After cooling down and storage at 7 °C, the hydrogel rode was extruded (Scheme S2).

*Formation process of hollow struct*ures: The gel rods prepared in the previous step were submerged into an iron chloride aqueous solution, and the cross-linking process started from the surface toward the center of the sample (Scheme S3). After immersion in solution for different durations, the hydrogels were cut to allow collection of the cross-sectional image. The hollow ratio was defined as A_{hollow}/A_{total} (A: area; Scheme S4).

Cell culture: Before cell culture, all samples were sterilized with 75 % alcohol and immersed in phosphate-buffered saline (PBS) to remove residual alcohol. The closed hollow fibers were used for encapsulation of cells. The cells were injected into the cavity of the fibers using a 20 G syringe. The samples were kept in a cell culture incubator, imaged after every 12 h, and kept in culture for 3–7 days. The cell culture medium was substituted with fresh medium every day. The cell viability and morphology were observed by a Zeiss LSM 880 confocal microscope after live/dead assay and immunofluorescence staining.

Acknowledgements

The authors acknowledge the National Natural Science Foundation of China (31800798, 51973023, 11774287, 11804275, and 21603026), the China Postdoctoral Science Foundation (2017M622997), Bundesministerium für Bildung und Forschung (BMBF) under an award number 031A360D, and the Max-Planck-Gesellschaft (Max Planck Partner Group UESTC-MPIP).

Conflict of interest

The authors declare no conflict of interest.

Keywords: gels · hollow interiors · hydrophobic effects · macroscopic self-evolution

How to cite: *Angew. Chem. Int. Ed.* **2020**, *59*, 5611 – 5625
Angew. Chem. **2020**, *132*, 5660 – 5664

[1] A. R. Studart, R. M. Erb, *Soft matter* **2014**, *10*, 1284 – 1294.
[2] H. Sun, C. P. Kabb, M. B. Sims, B. S. Sumerlin, *Prog. Polym. Sci.* **2019**, *89*, 61 – 75.
[3] P. Egan, R. Sinko, P. R. LeDuc, S. Keten, *Nat. Commun.* **2015**, *6*, 7418.
[4] C. Sanchez, H. Arribart, M. M. G. Guille, *Nat. Mater.* **2005**, *4*, 277.
[5] J. C. Cremaldi, B. Bhushan, *Beilstein J. Nanotechnol.* **2018**, *9*, 907 – 935.
[6] S. Vanneste, J. Friml, *Cell* **2009**, *136*, 1005 – 1016.
[7] Q. Guo, E. Dai, X. Han, S. Xie, E. Chao, Z. Chen, *J. R. Soc. Interface* **2015**, *12*, 20150598.
[8] W. G. van Doorn, U. van Meeteren, *J. Exp. Bot.* **2003**, *54*, 1801 – 1812.
[9] F. Apolinário, C. Martius, *Forest Ecol. Manag.* **2004**, *194*, 23 – 28.
[10] Z. Liu, M. A. Meyers, Z. Zhang, R. O. Ritchie, *Prog. Mater. Sci.* **2017**, *88*, 467 – 498.
[11] M. Samejima, T. Sibaoka, *Plant Cell Physiol.* **1980**, *21*, 467 – 479.
[12] S. A. van Rossum, M. Tena-Solsona, J. H. van Esch, R. Eelkema, J. Boekhoven, *Chem. Soc. Rev.* **2017**, *46*, 5519 – 5535.
[13] A. Lendlein, H. Jiang, O. Jünger, R. Langer, *Nature* **2005**, *434*, 879.
[14] T. Xie, *Nature* **2010**, *464*, 267.
[15] Y. Fang, Y. Ni, S.-Y. Leo, C. Taylor, V. Basile, P. Jiang, *Nat. Commun.* **2015**, *6*, 7416.
[16] T. J. White, D. J. Broer, *Nat. Mater.* **2015**, *14*, 1087.
[17] Z. Pei, Y. Yang, Q. Chen, Y. Wei, Y. Ji, *Adv. Mater.* **2016**, *28*, 156 – 160.
[18] T. Guin, M. J. Settle, B. A. Kowalski, A. D. Auguste, R. V. Beblo, G. W. Reich, T. J. White, *Nat. Commun.* **2018**, *9*, 2531.
[19] Y. Chen, A. M. Kushner, G. A. Williams, Z. Guan, *Nat. Chem.* **2012**, *4*, 467.
[20] R. J. Wojtecki, M. A. Meador, S. J. Rowan, *Nat. Mater.* **2011**, *10*, 14.
[21] A. K. Boal, F. Ilhan, J. E. DeRouchey, T. Thurn-Albrecht, T. P. Russell, V. M. Rotello, *Nature* **2000**, *404*, 746.
[22] S. Janbaz, R. Hedayati, A. Zadpoor, *Mater. Horiz.* **2016**, *3*, 536 – 547.
[23] A. R. Studart, *Chem. Soc. Rev.* **2016**, *45*, 359 – 376.
[24] X. Yin, Z. Liu, D. Wang, X. Pei, B. Yu, F. Zhou, *J. Bionic Eng.* **2015**, *12*, 1 – 16.
[25] A. Wang, W. Shi, J. Huang, Y. Yan, *Soft Matter* **2016**, *12*, 337 – 357.
[26] H. Che, S. Cao, J. C. van Hest, *J. Am. Chem. Soc.* **2018**, *140*, 5356 – 5359.
[27] E. Donath, S. Moya, B. Neu, G. B. Sukhorukov, R. Georgieva, A. Voigt, H. Bäumler, H. Kiesewetter, H. Möhwald, *Chem. Eur. J.* **2002**, *8*, 5481 – 5485.
[28] J. W. Pang, I. P. Bond, *Compos. Sci. Technol.* **2005**, *65*, 1791 – 1799.
[29] P. Lin, S. Ma, X. Wang, F. Zhou, *Adv. Mater.* **2015**, *27*, 2054 – 2059.
[30] J. H. Wang, *J. Phys. Chem.* **1965**, *69*, 4412 – 4412.
[31] P. Vanysek in *Ionic conductivity and diffusion at infinite dilution* (Ed.: D. R. Lide), CRC, Boca Raton, **2000**, chap. 5, p. 76 – 78.
[32] A. Vagias, P. Košovan, K. Koynov, C. Holm, H.-J. Butt, G. Fytas, *Macromolecules* **2014**, *47*, 5303 – 5312.
[33] Y. Jun, E. Kang, S. Chae, S.-H. Lee, *Lab Chip* **2014**, *14*, 2145 – 2160.
[34] H. Onoe, T. Okitsu, A. Itou, M. Kato-Negishi, R. Gojo, D. Kiriya, K. Sato, S. Miura, S. Iwanaga, K. Kuribayashi-Shigetomi, *Nat. Mater.* **2013**, *12*, 584.

Manuscript received: October 24, 2019
Revised manuscript received: November 29, 2019
Accepted manuscript online: December 15, 2019
Version of record online: January 29, 2020

